ACS Macro Letters

Letter

pubs.acs.org/macroletters

High-Performance All-Polymer Solar Cells Based on Face-On Stacked Polymer Blends with Low Interfacial Tension

Hyunbum Kang,† Ki-Hyun Kim,† Joonhyeong Choi, Changyeon Lee, and Bumjoon J. Kim*

Department of Chemical and Biomolecular Engineering, Korea Advanced Institute of Science and Technology (KAIST), Daejeon 305-701, Republic of Korea

Supporting Information

ABSTRACT: We report highly efficient all-polymer solar cells with power conversion efficiencies of over 4.5% by highly intermixed blends of PTB7-Th donor and P(NDI2OD-T2) acceptor polymers. The low interfacial tension and the face-on $\pi-\pi$ stackings of the all-polymer blends afforded desired nanophase morphology, which facilitates efficient charge transport from the active layer to each electrode. In addition, the incorporation of 1,8-diiodooctane additives was able to tune the degree of crystallinity and orientation of P(NDI2OD-T2) acceptors, resulting in remarkable enhancement of electron mobility, external quantum efficiency, and J_{SC} values.

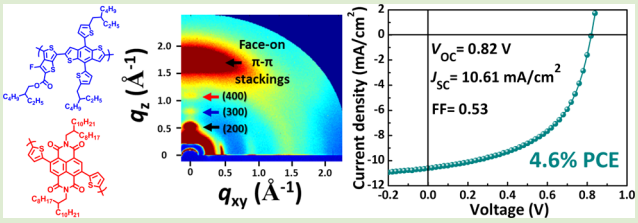

Extensive research activities have been focused on bulk-heterojunction (BHJ) type polymer solar cells (PSCs) because of their ease of fabrication, flexibility, and potential for cost-effective mass production.[1,2] The power conversion efficiency (PCE) of polymer/phenyl-C_{61}-butyric-acid-methyl-ester (PCBM)-based BHJ solar cells has increased dramatically up to 9−10% over the past decade with the development of low-bandgap materials[3−8] and advance of device architectures.[9−12] In recent years, great effort has also been devoted to replacing the conventional PCBM as an electron acceptor. For example, to increase the open-circuit voltage (V_{OC}) in polymer/fullerene based PSCs, new fullerene bisadducts with higher lowest unoccupied molecular orbital (LUMO) level than that of PCBM have been developed.[13−15] However, the fullerene acceptors have disadvantages, such as relatively weak absorption ability in the visible region due to their symmetrical structures; the need for high purity, making their synthesis very expensive; thermally unstable morphology of polymer/fullerene blend films due to the rapid diffusion of fullerene molecules; and restricted chemical and energetic tunability, which limits the design of complementary polymer donors for maximum PSC performance, in particular for enhancing the V_{OC} and short-circuit current (J_{SC}) simultaneously.[16−18]

All-polymer solar cells (all-PSCs), which consist of polymer donor/polymer acceptor blends, have potential advantages over typical polymer/fullerene systems, including enhanced absorption coefficients, the extensive tunability of their energetic and chemical properties, which result in simultaneously increased Voc and J_{SC} values, and superior chemical, thermal, and mechanical stabilities.[18−27] However, despite these attractive features of all-PSCs, less success has been realized for all-PSCs as compared to polymer/fullerene systems, with few systems exhibiting PCEs over 2%.[21,28−32] Only recently, two groups reported PCEs of over 4%.[20,22] These relatively low PCEs for all-PSCs are mainly due to the undesirable features of the BHJ blend morphology, including large-scale phase-separated domain size, inhomogeneous internal phase composition, and reduced ordering of polymer chains,[19,28,33−37] which limit the generation and transport of free charge carriers and, subsequently, the device performance. Also, the electron mobility of polymer acceptors is typically much lower than that of fullerene derivatives.

To address the above-mentioned issues and realize the high-performance all-PSCs, we need to identify well-matched polymer donor−acceptor pairs while simultaneously tuning the degree of phase separation and polymer crystallinity. More specifically, critical requirements include (1) well-aligned energy levels of polymer donors and acceptors for efficient charge separation; (2) favorable molecular interactions between two different polymers that lead to low interfacial tension at the donor−acceptor interface, thus producing well-mixed, interpenetrating networks of all-polymer blends; (3) desirable molecular ordering of two different polymers (i.e., face-on orientation) for facilitating efficient charge transport between the electrodes; and (4) highly crystalline polymer acceptors with high electron mobilities.[18,19,21] In this letter, we report on highly efficient all-PSCs by utilizing the low-bandgap polymer of poly[4,8-bis(5-(2-ethylhexyl)thiophen-2-yl)benzo[1,2-*b*:4,5-*b*′]dithiophene-*alt*-3-fluorothieno[3,4-*b*]thiophene-2-carboxylate] (PTB7-Th) as the electron donor[8,38] and poly[[*N*,*N*′-bis(2-octyldodecyl)-napthalene-1,4,5,8-bis(dicarboximide)-2,6-diyl]-*alt*-5,5′-(2,2′-bithiophene)] P(NDI2OD-T2) as the acceptor[20,39,40] (Scheme 1). PTB7-Th (number-average molecular weight (M_n) = 24 kg/mol, Table 1) exhibits higher

Received: July 10, 2014
Accepted: September 4, 2014
Published: September 16, 2014

   dx.doi.org/10.1021/mz500415a | *ACS Macro Lett.* 2014, 3, 1009−1014

Scheme 1. Schematic Illustration of Our Highly Efficient All-PSC System Based on Well-Intermixed and Face-On Stacked Polymer Blends. Chemical Structures and Absorption Coefficients (UV−vis Spectra) of the PTB7-Th Donor Polymer, P(NDI2OD-T2) Acceptor Polymer, and Their Blends Used in Our Study

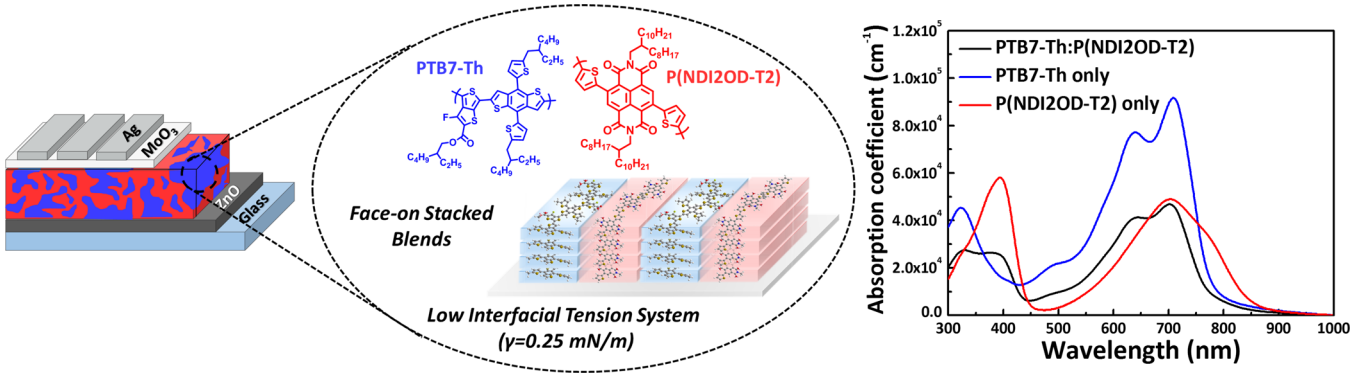

absorption coefficient (~10^5 cm^{-1}) than the well-known PTB7 polymer (Figure S1, Supporting Information).

Table 1. Polymer Information Used in This Study

polymer information	M_n/M_w (kg/mol)[a]	PDI (M_w/M_n)[a]	E_g^{opt} (eV)[b]	surface tension[c] (mN/m)
PTB7-Th	24/76	3.10	1.60	26.1
P(NDI2OD-T2)	32/79	2.40	1.50	25.5

[a]The molecular weights and polydispersity index (PDI) of the polymers were determined by GPC using *o*-DCB as the eluent at 80 °C calibrated by standard PS. [b]Determined by UV−vis absorption onsets in the polymer films. [c]Determined by contact angle measurements.

Also, the range of the absorption band of PTB7-Th (500−775 nm) is extended beyond that of PTB7 (500−750 nm) by 25 nm toward longer wavelengths. P(NDI2OD-T2) (M_n = 32 kg/mol, Table 1) was synthesized and used as the n-type polymer because of its high electron mobility and electron affinity and light absorption ability at near-IR wavelengths, as shown in Scheme 1. It was also noted that the PTB7-Th and P(NDI2OD-T2) polymers have the LUMO/HOMO levels of −3.6 eV/−5.2 eV and −4.3 eV/−5.9 eV, respectively,[20,38] which produce well-matched energy alignment with the energy offsets of LUMO−LUMO (0.7 eV) and HOMO−HOMO (0.7 eV) that are sufficient to generate free charges at the PTB7-Th/P(NDI2OD-T2) interfaces.[41−43] More importantly, the PTB7-Th and P(NDI2OD-T2) have very similar surface tensions of 26.1 and 25.5 mN/m, respectively, as measured by contact angle experiments (Table 1 and Figure S2 and Table S1, Supporting Information). Therefore, polymer blends could have the potential for forming the well-intermixed morphology with suppressed phase separation due to the extremely low interfacial tension of 0.25 mN/m between the PTB7-Th and P(NDI2OD-T2) domains, as summarized in Table S1 (Supporting Information). For reference, this value is only 4% of the interfacial tension of 7.9 mN/m between poly(3-hexylthiophene) (P3HT) and P(NDI2OD-T2).[24,44] Finally, both the PTB7-Th and P(NDI2OD-T2) polymers have strong face-on $\pi-\pi$ stackings, which are favorable for hole and electron transport, respectively, between the electrodes.

To explore the potential of the PTB7-Th/P(NDI2OD-T2) blend system for all-PSCs, we fabricated both normal-type (n-all-PSCs) and inverted-type all-PSCs (i-all-PSCs). (The detailed procedure for device structure and fabrication is described in the Supporting Information.) The optimized donor:acceptor (D:A) blend ratio was 1.3:1 (w/w), and the optimized film thickness of the BHJ type PTB7-Th:P(NDI2OD-T2) layer was about 110−120 nm. Figure 1 shows

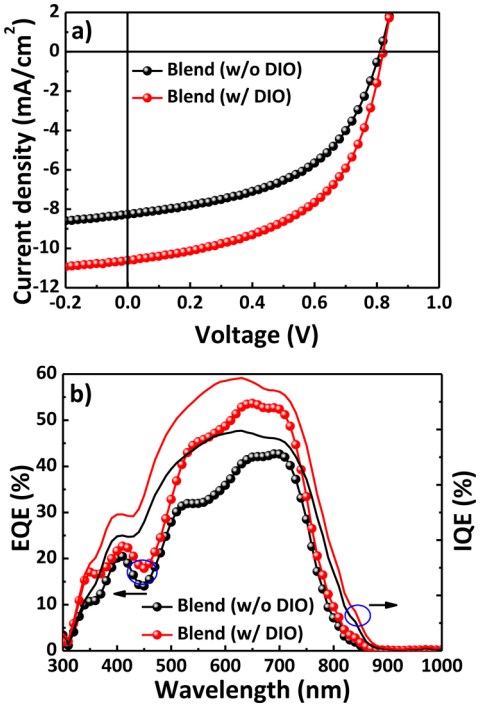

Figure 1. (a) Optimized *J*−*V* characteristics of PTB7-Th:P(NDI2OD-T2)-based i-all-PSCs and (b) EQE and IQE (EQE/device absorbance) spectra of optimized devices with and without DIO.

the optimized *J*−*V* curves, the external quantum efficiency (EQE) spectra, and the internal quantum efficiency (IQE) spectra of i-all-PSCs with and without the solvent additives of 1,8-diiodooctane (DIO), and the optimized photovoltaic parameters of i-all-PSCs are summarized in Table 2. The characteristics of i-all-PSC and n-all-PSC devices with other fabrication conditions (i.e., different volumetric ratios of DIO additives) are listed in Tables S2 and S3 (Supporting Information), respectively. In addition, the optimized *J*−*V* curves and EQE spectra of n-all-PSCs are shown in Figure S3 (Supporting Information). The best PCE value of i-all-PSCs of

dx.doi.org/10.1021/mz500415a | ACS Macro Lett. 2014, 3, 1009−1014

Table 2. Photovoltaic Parameters of the PTB7-Th:P(NDI2OD-T2)-Based i-all-PSC Devices without and with DIO

inverted type	V_{oc} (V)	J_{sc} (mA cm^{-2})	FF	PCE_{max} (%)	EQE_{max} (%)	IQE_{max} (%)	calcd J_{sc} (mA cm^{-2})
w/o DIO	0.810	8.27	0.51	3.41[a]	42.7	47.7	8.01
w/DIO	0.821	10.61	0.53	4.60[b]	53.6	59.2	10.30

[a]The average PCE value of the devices was 3.32%. [b]The average PCE value of the devices was 4.48%.

PTB7-Th:P(NDI2OD-T2) without any solvent additives was 3.41% (V_{OC}: 0.81 V, J_{SC}: 8.27 mA cm^{-2}, and FF: 0.51).

When a small amount of DIO (1.25 vol %) was added into all-polymer blends, the best PCE value increased dramatically to 4.60% (V_{OC}: 0.82 V, J_{SC}: 10.61 mA cm^{-2}, and FF: 0.53), which represents one of the highest efficiencies of all-PSCs reported to date. It is interesting to notice that both the devices without and with DIO additives showed high FF value over 0.5, suggesting the formation of a well-optimized, bicontinuous network of the donor and acceptor domains as a result of their low interfacial interaction. The PCE values changed with different amounts of DIO additives (ranging from 0.5 to 1.5 vol %), but the PCE values still were greater than that of the device without DIO additives (Table S2, Supporting Information). A similar trend in the performance of n-all-PSCs was also observed when the DIO additives were used (Table S3, Supporting Information). In addition, we have fabricated PTB7:P(NDI2OD-T2) devices as the control, to validate the high photovoltaic performance of our PTB7-Th:P(NDI2OD-T2)-based all-PSC system (Table S4, Supporting Information). The PCE values of the optimized PTB7:P(NDI2OD-T2)-based all-PSCs that were made with 1 vol % of DIO additives were obtained as 2.54% (V_{OC}: 0.807 V, J_{SC}: 7.12 mA cm^{-2}, and FF: 0.44), which agreed well with the values reported previously.[21] Thus, the PTB7-Th was beneficial in producing high performance all-PSC devices.

The significant enhancement of the PCE values in PTB7-Th:P(NDI2OD-T2)-based all-PSCs by using DIO additives was mainly attributed to the improvement in the J_{SC} value by 28% (from 8.27 to 10.61 mA cm^{-2}). The EQE and IQE values were measured to evaluate the spectral responses of the all-PSCs. It is evident that the J_{SC} enhancements were well reflected in the changes of the EQE and IQE values, showing 25% and 24% increases, respectively (Figure 1b). For example, the EQE_{max} values of the optimized PTB7-Th:P(NDI2OD-T2)-based i-all-PSCs were improved by DIO additives from 42.7% to 53.6%. The IQE values were calculated by dividing the EQE values by the fraction of photons absorbed in the active layer,[45] and these values also showed a significant enhancement from 47.7% to 59.2%. To address the origin of IQE enhancement in the all-PSCs by using DIO additives, the electrical properties of the PTB7-Th:P(NDI2OD-T2) devices without and with DIO were compared by measuring the electric-field-dependent current densities of the devices at optimized device conditions under reverse bias from 0 to −10 V (Figure S4, Supporting Information). The stronger field dependence (large slope of the $J-V$ curve) indicated that the charge collection process in all-PSC devices (i.e., charge transport) was less efficient.[46] Interestingly, the average slopes (**S**) of the $J-V$ curves for both the n-all-PSCs and the i-all-PSCs were reduced by addition of the DIO. For example, the **S** value for n-all-PSC devices was significantly decreased from 1.6 to 1.1 by adding 0.5 vol % of the DIO additives, while the PCE value of the devices was increased from 2.39 to 4.21%.

To gain a deeper insight into the changes in the electrical properties of the all-PSCs caused by the DIO additives, we measured the charge-carrier mobilities in the PTB7-Th:P(NDI2OD-T2) devices with and without DIO. The hole mobility (μ_h) and electron mobility (μ_e) in both the polymer only and the all-polymer blend films were measured and compared using the space-charge-limited current (SCLC) method as shown in Figure S5 (Supporting Information) and Table 3. It was observed that the measured hole mobilities of

Table 3. Hole and Electron Mobility Values of the Polymer Neat and the All-Polymer Blends Measured by the SCLC Method

sample	μ_h (cm^2/V s)	μ_e (cm^2/V s)
PTB7-Th only	9.6×10^{-5}	-
P(NDI2OD-T2) only	-	1.1×10^{-5}
PTB7-Th:P(NDI2OD-T2) (w/o DIO)	3.7×10^{-4}	5.3×10^{-7}
PTB7-Th:P(NDI2OD-T2) (w/DIO)	4.2×10^{-4}	6.7×10^{-6}

PTB7-Th only and all-polymer blends (with and without DIO (w/and w/o DIO)) were approximately the same, i.e., on the order of 10^{-4} cm^2/V s. In contrast, there were remarkable differences in the electron mobilities between the P(NDI2OD-T2) only and the all-polymer blends. The electron mobility of the PTB7-Th:P(NDI2OD-T2) (w/o DIO) devices (5.3×10^{-7} cm^2/V s) was only about 5% of that of the P(NDI2OD-T2) only film (1.1×10^{-5} cm^2/V s). This suggested that the morphological behavior of P(NDI2OD-T2) domains, including their crystalline behavior, was largely disrupted by the presence of PTB7-Th donors in the blends.[47] Interestingly, when a small amount of DIO was added into the all-polymer blends, the electron mobility (6.7×10^{-6} cm^2/V s) was dramatically increased by a factor of more than 10, and consequently, the ratio between hole and electron mobilities in the device with DIO was more balanced. Thus, this significant improvement in charge transport efficiency is a key parameter for improving the transport of the electrons to the electrode and for reducing charge recombination, resulting in the higher J_{SC} and FF values in the all-PSC devices.

To investigate the changes in the electrical properties of the BHJ PSCs induced by the DIO additives, first we examined the blend morphologies of PTB7-Th:P(NDI2OD-T2) w/ and w/o DIO by using tapping-mode atomic force microscopy (AFM) images (Figure S6, Supporting Information). Although the images of the both samples showed bicontinuous structures of polymer blends with relatively small-length scale domain favorable for exciton dissociation, the value of the RMS surface roughness increased from 1.3 nm for the sample w/o DIO to 1.9 nm for the sample w/ DIO. This was attributed mainly to the fact that the DIO additives, which have a high boiling point (333 °C), allowed the film to dry for a longer time, resulting in the development of more phase separation in the all-polymer blends.[17,48] Next, steady-state photoluminescence (PL) measurements were performed.[20,46] The intensities of PL spectra from PTB7-Th to P(NDI2OD-2T) of the all-polymer blend films w/ and w/o DIO additives were compared, both of which were measured by excitation at a wavelength of 640 nm. Figure

dx.doi.org/10.1021/mz500415a | ACS Macro Lett. 2014, 3, 1009−1014

S7 (Supporting Information) shows dramatic PL quenching in both the blend films w/ and w/o DIO additives compared to the pristine PTB7-Th film. Interestingly, the degree of the emission quenchings for the blend film w/o DIO additives was rather high (96%) compared to that for the film w/DIO (90%), which supports the morphological trends of PTB7-Th:P(NDI2OD-T2) blend films by AFM measurements. Although the DIO additives induced more phase separation between the PTB7-Th:P(NDI2OD-T2) domains, the degree of phase separation was still sufficient to produce efficient charge separation and transport. From the combined results of the PL quenching study and the AFM measurements, the difference in the macroscopic aspect of the blend morphology (i.e., the length scale of the phase-separated domains) was not the main reason for the significant enhancements in J_{SC} value by addition of DIO in our all-PSC devices.

Direct evidence for the changes of the electrical properties and the PCE values of all-PSCs can be gleaned by examination of the microstructure of all-polymer blends via grazing incidence X-ray scattering (GIXS) (Figure 2). While Figures 2a and b present the GIXS patterns of the pristine P(NDI2OD-T2) and PTB7-Th polymer films, Figures 2c and d show the GIXS patterns of the PTB7-Th/P(NDI2OD-T2) blend films w/o and w/DIO additives, respectively. The PTB7-Th/P(NDI2OD-T2) blend films were prepared identically to the best device conditions. First, Figure 2a,b and Figure S8 (Supporting Information) show that PTB7-Th and P(NDI2OD-T2) polymer thin films have distinct peaks of reflections from the (100) crystal plane that represent similar lamellar spacings of 2.3 nm (q_{in} = 0.27 Å^{-1}) and 2.5 nm (q_{in} = 0.25 Å^{-1}), respectively. In particular, as shown in Figures 2a, b, and e, both the PTB7-Th and P(NDI2OD-T2) polymer thin films have strong (010) peaks of $\pi-\pi$ stackings with very similar spacing of ~0.40 nm in the out-of-plane X-ray profile, which indicates that both polymer backbones adopt a preferential face-on orientation relative to the substrate. These combinations of face-on stacked polymer donor and acceptor should be beneficial for charge transport from the active layer to the corresponding electrodes, which could be one of the reasons for the high PCE value of the all-PSCs.[24] It is worthwhile to note that whereas the P(NDI2OD-T2) film showed strong (100), (200), and (300) peaks with much more pronounced reflections in both the in-plane and out-of-plane directions, the PTB7-Th film exhibited the only first-order scattering of a (100) peak; this result indicates that the P(NDI2OD-T2) stacks in the film exhibited a highly ordered structural organization due to their strong crystalline behavior. However, the crystalline feature of P(NDI2OD-T2) was suppressed and disrupted significantly by the blending of PTB7-Th polymers, as evidenced in the disappearance of high-order peaks (i.e., (200) and (300)) in the PTB7-Th/P(NDI2OD-T2) blend w/o DIO (Figures 2c and e). In contrast, when small amounts of DIO additives were added into the all-PSCs, the crystalline nature of P(NDI2OD-T2) polymers was recovered completely with the appearance of highly ordered structures up to the fourth-order (400) peaks (Figures 2d and e). In addition, the PTB7-Th/P(NDI2OD-T2) w/DIO showed a much more prominent $\pi-\pi$ stacking peak with face-on geometry compared to those in the blend w/o DIO. These trends were supported further by the GIXS patterns of the P(NDI2OD-T2) only film and the PTB7-Th only film w/ and w/o DIO (Figure S9, Supporting Information). The addition of DIO induced a significant

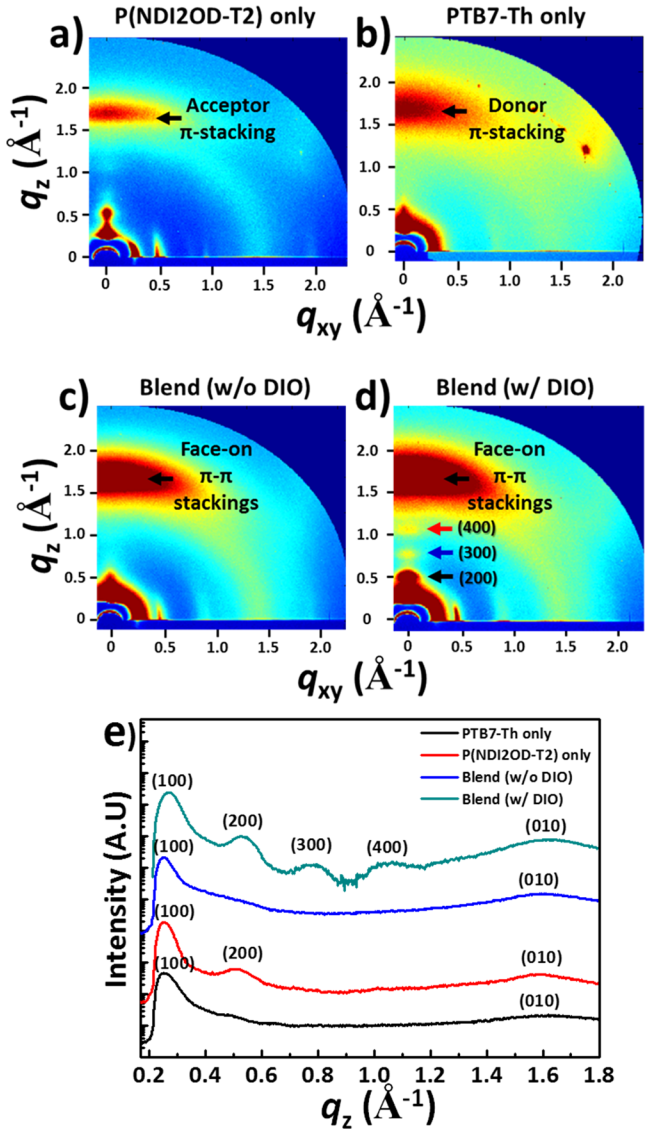

Figure 2. 2D GIXS images for (a) P(NDI2OD-T2) only film, (b) PTB7-Th only film, (c) PTB7-Th:P(NDI2OD-T2) blend film without DIO, and (d) the blend with DIO. (e) Linecut of GIXS images in the out-of-plane of the indicated polymer-only films and PTB7-Th:P(NDI2OD-T2) blend films w/o and w/DIO.

enhancement in the crystallinity of P(NDI2OD-T2), whereas the effect on the structure of PTB7-Th film was almost negligible.[17] Thus, a dramatic change in the microstructures of P(NDI2OD-T2), including the recovery of the strong crystalline feature of P(NDI2OD-T2) and its strong face-on $\pi-\pi$ stacking in the PTB7-Th/P(NDI2OD-T2) blends, induced remarkable improvement of the electron mobilities of more than 1 order of magnitude in the all-PSCs, as shown in Table 3, and this produced a balanced hole/electron mobility, resulting in higher J_{SC} and FF values. Very recently, Mori et al. reported PTB7-Th and P(NDI2OD-T2) polymer-based all-PSCs with PCE value of 5.7%.[49] However, it is worthwhile to note that the optimal condition for our device was very different from that of the reported work. For example, in our work, the solvent additive was to be very important in optimizing the device performance by enhancing the crystalline order of the P(NDI2OD-T2) acceptors and their electron mobilities.

dx.doi.org/10.1021/mz500415a | ACS Macro Lett. 2014, 3, 1009−1014

In conclusion, we demonstrated highly efficient all-PSCs with PCEs of over 4.5% by using highly intermixed blends of PTB7-Th and P(NDI2OD-T2) with low interfacial tension. A desired nanophase morphology with face-on $\pi-\pi$ stackings of the PTB7-Th and P(NDI2OD-T2) blends was well realized in the optimized devices. This optimal morphology is one of the keys to facilitate efficient charge transport to each electrode and produces high J_{SC} values (>10 mA cm^{-2}) and FF values (>0.5) in i-all-PSCs (PCE = 4.60%), which are among the highest values reported for all-PSCs. The role of DIO additives on the enhancement of the PSC performance was identified. In particular, the crystalline characteristics of P(NDI2OD-T2) electron acceptors were dramatically enhanced with the appearance of highly ordered polymer organizations with face-on geometry, as evidenced by GIXS measurements. Engineering the degree of crystallinity and orientation of P(NDI2OD-T2) enhanced the electron mobility remarkably, producing 25% improvements in the EQE and J_{SC} values. Our findings from this model system provide guidelines for the choice of polymer blends for highly efficient all-PSCs, particularly in both macro- and microscopic aspects of blend morphology.

■ ASSOCIATED CONTENT

Ⓢ Supporting Information

Materials and methods, detailed experimental procedures, and additional data. This material is available free of charge via the Internet at http://pubs.acs.org.

■ AUTHOR INFORMATION

Corresponding Author

*E-mail: bumjoonkim@kaist.ac.kr.

Author Contributions

†These authors contributed equally.

Notes

The authors declare no competing financial interest.

■ ACKNOWLEDGMENTS

This research was supported by the National Research Foundation Grant (2012M1A2A2671746, 2013R1A2A1A03069803), funded by the Korean Government. This research was supported by the New & Renewable Energy Program of KETEP Grant (20133030000130, 20133030011330), funded by the Ministry of Trade, Industry & Energy, Republic of Korea. The authors also acknowledge the Research Project of the KAIST EEWS Initiative (EEWSN01140052) for the financial support. We also thank Ms. Seonju Jeong and Prof. Jung-Yong Lee for the assistance with EQE and IQE measurements.

■ REFERENCES

(1) Yu, G.; Gao, J.; Hummelen, J. C.; Wudl, F.; Heeger, A. J. *Science* **1995**, *270*, 1789−1791.

(2) Søndergaard, R.; Hösel, M.; Angmo, D.; Larsen-Olsen, T. T.; Krebs, F. C. *Mater. Today* **2012**, *15*, 36−49.

(3) Zhong, H.; Li, Z.; Deledalle, F.; Fregoso, E. C.; Shahid, M.; Fei, Z.; Nielsen, C. B.; Yaacobi-Gross, N.; Rossbauer, S.; Anthopoulos, T. D.; Durrant, J. R.; Heeney, M. *J. Am. Chem. Soc.* **2013**, *135*, 2040−2043.

(4) Zhang, M.; Guo, X.; Zhang, S.; Hou, J. *Adv. Mater.* **2014**, *26*, 1118−1123.

(5) Cabanetos, C.; El Labban, A.; Bartelt, J. A.; Douglas, J. D.; Mateker, W. R.; Fréchet, J. M. J.; McGehee, M. D.; Beaujuge, P. M. *J. Am. Chem. Soc.* **2013**, *135*, 4656−4659.

(6) Hendriks, K. H.; Heintges, G. H. L.; Gevaerts, V. S.; Wienk, M. M.; Janssen, R. A. J. *Angew. Chem., Int. Ed.* **2013**, *52*, 8341−8344.

(7) Kang, T. E.; Cho, H.-H.; Kim, H. j.; Lee, W.; Kang, H.; Kim, B. J. *Macromolecules* **2013**, *46*, 6806−6813.

(8) Liang, Y.; Xu, Z.; Xia, J.; Tsai, S.-T.; Wu, Y.; Li, G.; Ray, C.; Yu, L. *Adv. Mater.* **2010**, *22*, E135−E138.

(9) Kim, J. Y.; Lee, K.; Coates, N. E.; Moses, D.; Nguyen, T.-Q.; Dante, M.; Heeger, A. J. *Science* **2007**, *317*, 222−225.

(10) Dou, L. T.; You, J. B.; Yang, J.; Chen, C. C.; He, Y. J.; Murase, S.; Moriarty, T.; Emery, K.; Li, G.; Yang, Y. *Nat. Photonics* **2012**, *6*, 180−185.

(11) Na, S.-I.; Kim, S.-S.; Jo, J.; Oh, S.-H.; Kim, J.; Kim, D.-Y. *Adv. Funct. Mater.* **2008**, *18*, 3956−3963.

(12) Li, X.; Choy, W. C. H.; Huo, L.; Xie, F.; Sha, W. E. I.; Ding, B.; Guo, X.; Li, Y.; Hou, J.; You, J.; Yang, Y. *Adv. Mater.* **2012**, *24*, 3046−3052.

(13) He, Y.; Chen, H.-Y.; Hou, J.; Li, Y. *J. Am. Chem. Soc.* **2010**, *132*, 1377−1382.

(14) Kim, K.-H.; Kang, H.; Nam, S. Y.; Jung, J.; Kim, P. S.; Cho, C.-H.; Lee, C.; Yoon, S. C.; Kim, B. J. *Chem. Mater.* **2011**, *23*, 5090−5095.

(15) Lenes, M.; Wetzelaer, G.-J. A. H.; Kooistra, F. B.; Veenstra, S. C.; Hummelen, J. C.; Blom, P. W. M. *Adv. Mater.* **2008**, *20*, 2116−2119.

(16) Jung, I. H.; Lo, W.-Y.; Jang, J.; Chen, W.; Zhao, D.; Landry, E. S.; Lu, L.; Talapin, D. V.; Yu, L. *Chem. Mater.* **2014**, *26*, 3450−3459.

(17) Zhou, E.; Cong, J.; Hashimoto, K.; Tajima, K. *Adv. Mater.* **2013**, *25*, 6991−6996.

(18) Facchetti, A. *Mater. Today* **2013**, *16*, 123−132.

(19) McNeill, C. R. *Energy Environ. Sci.* **2012**, *5*, 5653−5667.

(20) Mori, D.; Benten, H.; Okada, I.; Ohkita, H.; Ito, S. *Adv. Energy Mater.* **2014**, DOI: 10.1002/aenm.201301006.

(21) Zhou, N.; Lin, H.; Lou, S. J.; Yu, X.; Guo, P.; Manley, E. F.; Loser, S.; Hartnett, P.; Huang, H.; Wasielewski, M. R.; Chen, L. X.; Chang, R. P. H.; Facchetti, A.; Marks, T. J. *Adv. Energy Mater.* **2014**, DOI: 10.1002/aenm.201300785.

(22) Zhou, Y.; Kurosawa, T.; Ma, W.; Guo, Y.; Fang, L.; Vandewal, K.; Diao, Y.; Wang, C.; Yan, Q.; Reinspach, J.; Mei, J.; Appleton, A. L.; Koleilat, G. I.; Gao, Y.; Mannsfeld, S. C. B.; Salleo, A.; Ade, H.; Zhao, D.; Bao, Z. *Adv. Mater.* **2014**, *26*, 3767−3772.

(23) Earmme, T.; Hwang, Y.-J.; Murari, N. M.; Subramaniyan, S.; Jenekhe, S. A. *J. Am. Chem. Soc.* **2013**, *135*, 14960−14963.

(24) Schubert, M.; Collins, B. A.; Mangold, H.; Howard, I. A.; Schindler, W.; Vandewal, K.; Roland, S.; Behrends, J.; Kraffert, F.; Steyrleuthner, R.; Chen, Z.; Fostiropoulos, K.; Bittl, R.; Salleo, A.; Facchetti, A.; Laquai, F.; Ade, H. W.; Neher, D. *Adv. Funct. Mater.* **2014**, *24*, 4068−4081.

(25) Huang, H.; Zhou, N.; Ortiz, R. P.; Chen, Z.; Loser, S.; Zhang, S.; Guo, X.; Casado, J.; López Navarrete, J. T.; Yu, X.; Facchetti, A.; Marks, T. J. *Adv. Funct. Mater.* **2014**, *24*, 2782−2793.

(26) Kim, Y.; Lim, E. *Polymers* **2014**, *6*, 382−407.

(27) Cheng, P.; Ye, L.; Zhao, X.; Hou, J.; Li, Y.; Zhan, X. *Energy Environ. Sci.* **2014**, *7*, 1351−1356.

(28) Mori, D.; Benten, H.; Ohkita, H.; Ito, S.; Miyake, K. *ACS Appl. Mater. Interfaces* **2012**, *4*, 3325−3329.

(29) Mori, D.; Benten, H.; Kosaka, J.; Ohkita, H.; Ito, S.; Miyake, K. *ACS Appl. Mater. Interfaces* **2011**, *3*, 2924−2927.

(30) Zhou, Y.; Yan, Q.; Zheng, Y.-Q.; Wang, J.-Y.; Zhao, D.; Pei, J. *J. Mater. Chem. A* **2013**, *1*, 6609−6613.

(31) Holcombe, T. W.; Woo, C. H.; Kavulak, D. F. J.; Thompson, B. C.; Fréchet, J. M. J. *J. Am. Chem. Soc.* **2009**, *131*, 14160−14161.

(32) Li, W.; Roelofs, W. S. C.; Turbiez, M.; Wienk, M. M.; Janssen, R. A. J. *Adv. Mater.* **2014**, *26*, 3304−3309.

(33) McNeill, C. R.; Greenham, N. C. *Adv. Mater.* **2009**, *21*, 3840−3850.

(34) Yan, H.; Collins, B. A.; Gann, E.; Wang, C.; Ade, H.; McNeill, C. R. *ACS Nano* **2011**, *6*, 677−688.

(35) Schubert, M.; Dolfen, D.; Frisch, J.; Roland, S.; Steyrleuthner, R.; Stiller, B.; Chen, Z.; Scherf, U.; Koch, N.; Facchetti, A.; Neher, D. *Adv. Energy Mater.* **2012**, *2*, 369−380.
(36) Swaraj, S.; Wang, C.; Yan, H.; Watts, B.; Lüning, J.; McNeill, C. R.; Ade, H. *Nano Lett.* **2010**, *10*, 2863−2869.
(37) McNeill, C. R.; Westenhoff, S.; Groves, C.; Friend, R. H.; Greenham, N. C. *J. Phys. Chem. C* **2007**, *111*, 19153−19160.
(38) Liao, S.-H.; Jhuo, H.-J.; Cheng, Y.-S.; Chen, S.-A. *Adv. Mater.* **2013**, *25*, 4766−4771.
(39) Yan, H.; Chen, Z. H.; Zheng, Y.; Newman, C.; Quinn, J. R.; Dotz, F.; Kastler, M.; Facchetti, A. *Nature* **2009**, *457*, 679−U671.
(40) Steyrleuthner, R.; Schubert, M.; Jaiser, F.; Blakesley, J. C.; Chen, Z.; Facchetti, A.; Neher, D. *Adv. Mater.* **2010**, *22*, 2799−2803.
(41) Kang, T. E.; Cho, H.-H.; Cho, C.-H.; Kim, K.-H.; Kang, H.; Lee, M.; Lee, S.; Kim, B.; Im, C.; Kim, B. J. *ACS Appl. Mater. Interfaces* **2013**, *5*, 861−868.
(42) Dennler, G.; Scharber, M. C.; Brabec, C. J. *Adv. Mater.* **2009**, *21*, 1323−1338.
(43) Veldman, D.; Meskers, S. C. J.; Janssen, R. A. J. *Adv. Funct. Mater.* **2009**, *19*, 1939−1948.
(44) Kim, K.-H.; Kang, H.; Kim, H. J.; Kim, P. S.; Yoon, S. C.; Kim, B. J. *Chem. Mater.* **2012**, *24*, 2373−2381.
(45) Park, S. H.; Roy, A.; Beaupre, S.; Cho, S.; Coates, N.; Moon, J. S.; Moses, D.; Leclerc, M.; Lee, K.; Heeger, A. J. *Nat. Photonics* **2009**, *3*, 297−U295.
(46) Bloking, J. T.; Giovenzana, T.; Higgs, A. T.; Ponec, A. J.; Hoke, E. T.; Vandewal, K.; Ko, S.; Bao, Z.; Sellinger, A.; McGehee, M. D. *Adv. Energy. Mater.* **2014**, DOI: 10.1002/aenm.201301426.
(47) Mandoc, M. M.; Veurman, W.; Koster, L. J. A.; Koetse, M. M.; Sweelssen, J.; de Boer, B.; Blom, P. W. M. *J. Appl. Phys.* **2007**, *101*, 104512.
(48) Liu, X.; Huettner, S.; Rong, Z.; Sommer, M.; Friend, R. H. *Adv. Mater.* **2012**, *24*, 669−674.
(49) Mori, D.; Benten, H.; Okada, I.; Ohkita, H.; Ito, S. *Energy Environ. Sci.* **2014**, *7*, 2939−2943.